New Small Wheel Low-Voltage Power: Design Review

Jon Ameel[a], Dan Amidei[a], Karishma Sekhon Edgar[a], **Ryan Edgar**[a],
Yunjie Yang[a], Paolo Cova[b,f], Nicola Delmonte[b,f], Agostino Lanza[b],
Stefania Baccaro[c], Salvatore Fiore[c],
Mauro Citterio[d], Stefano Latorre[d], Massimo Lazzaroni[d,e]

[a]University of Michigan, Ann Arbor

[b]Istituto Nazionale di Fisica Nucleare di Pavia

[c] ENEA and INFN Sez di Roma

[d]Istituto Nazionale di Fisica Nucleare di Milano

[e]Università degli Studi di Milano

[f]Università degli Studi di Parma

February 5, 2015

1 Introduction

This document details the present status of research and development for the low-voltage power systems of the ATLAS New Small Wheel (NSW). The combination of large power requirements and low available cabling space suggests a point-of-load conversion architecture, where power is delivered to a front-end board (FEB) at a relatively high voltage (10 V or more) and then reduced to the delivery voltage by on-FEB power electronics.

This is potentially a multi-step process. Power will be delivered to the rim of the NSW at a voltage of at least 24 V. From the rim, it will be distributed to the individual front-end boards. If the FEBs are unable to directly accept the voltage delivered to the rim, an additional conversion step is required at the point of distribution. This point of distribution is also a natural location for circuit protection and ballast resistors. On the FEBs, power conversion will be accomplished by single-inductor buck converters, optionally followed by one or more low-dropout regulators (LDOs) for noise reduction or to provide additional output voltages.

The challenges in this approach are to ensure that the selected power conversion device(s) will:

1. Survive in the radiation and magnetic field environment of the NSW;
2. Effectively couple to the proposed cooling system;
3. Not introduce noise that may impact sensitive analog components;

4. Fit within the relatively small available space on the FEBs;

5. Allow a cabling solution that fits within the available space for services.

This material is written primarily with reference to the MicroMegas, although it is recognized that the chosen solution will likely be adopted by the sTGC detector as well.

2 Power Requirements and Design Constraints

The 7,500 front-end boards of the New Small Wheel are expected to require some 80 kW of delivered power (Tables 1b, 1a). Some 80% of this is for analog processing and digitization (i.e. the VMM). The balance is required by communications and logic. The power demands are almost exclusively at very low voltages (1.2 V or 1.5 V).

The estimated power consumption of individual FE boards are shown in Table 1a. These estimates are based on the expected power consumption of the major components on each board and an assumed average power-conversion efficiency of 64%. In the case of ASICs whose development is not yet advanced, these values are speculative. The remainder are taken from datasheets, or when possible from actual test results. Note that the pad trigger board is not included.

2.1 Radiation Load and Magnetic Field

The New Small Wheel is located sufficiently close to the interaction point that the radiation exposure is substantial over the NSW's design lifetime. Ten-year radiation loads at the inner and outer radii of the NSW are summarized in Table 2; the inner radius of the detector is subject to some $20 - 30\times$ the radiation load of the outer radius.

Additionally, the New Small Wheel is within the fringing fields of the toroidal bending magnets. These are very well-understood from particle tracking studies. In the NSW volume, the field ranges from negligible (inner radius) to over 5 kG (large sector corners). The majority of the NSW is subject to a field of less than 3 kG. This field is highly nonuniform; it is predominantly radial at high radii, but at intermediate radii becomes dominated by z and ϕ components.

2.2 Noise

On-detector power electronics are located within an extremely noise-sensitive environment. The analog electronics require particular consideration, but the density of the final installation and the potential for either conducted or radiated coupling between adjacent electronics mandates that any additional noise from power conversion be minimized.

Traditionally, noise is minimized by a combination of heavy passive filtering and a two-stage conversion process, where a DC-DC converter is followed by an LDO. The LDO provides regulation and active attenuation of the high-frequency noise from the DC-DC converter. Including a LDO stage, however, has a negative impact on the overall power conversion efficiency and entails the use of a further radiation-hard part. For that

Assumed Board Composition for Power Estimates

Part	Power (Watts)	Qty. Per Board: MMFE	ADDC	L1DDC	Strip	Pad	Router[1]	Pad Trigger
VMM	0.840	8			5-7	2-3		
RO ASIC	0.630	1			1	1		
TDS ASIC	1.000				3-4	1-2		
ART ASIC	0.500		2					
SCA	0.250	1			1	1		
GBTX	2.200		2	1				
GBTIA	0.250			1				
GBTLD	0.325		2	1				
Current at 1.2 V		5.60	0.83	-	3.50	1.40		
					4.90	2.10		
Current at 1.5 V		0.59	2.93	1.47	2.09	1.25		
					2.51	1.67		
Current at 2.5 V		?	0.26	0.23	?	?		
Total Power (Watts)		**7.60**	**6.05**	**2.78**	**7.34** **-9.65**	**3.56** **-5.03**	**16.00**	**10.00**

[1] Voltage rails for router: 1.0 V (x3), 1.2 V, 1.8 V, 2.5 V, 3.3 V

(a)

New Small Wheel Power Requirements

Device	Number of Devices	Power[1] (Watts)
MM		
MMFE	4096	11.88
ADDC	512	9.45
L1DDC	512	4.34
Total Power		**55700**
sTGC		
Strip (5 VMM)	128	11.47
Strip (6 VMM)	384	12.78
Strip (7 VMM)	256	15.08
Pad+Wire (2 VMM)	512	7.86
Pad+Wire (3 VMM)	256	5.56
L1DDC	512	4.34
Router	256	25.00
Pad Trigger	32	15.63
Total Power		**23716**

[1] Assuming a 64% on-FEB conversion efficiency.

(b)

Table 1: Estimates for FE board power consumption. Table (a) shows the estimate for each FEB. For those sTGC boards that accommodate different numbers of VMMs, multiple power estimates are shown. Also shown are estimates for the required current on each voltage rail. These estimates assume a worst-case scenario where the RO companion and SCA chip both draw primarily 1.5 V. Table (b) shows the total power consumption of the NSW derived from these estimates. These numbers assume a 64% average efficiency for on-board power conversion; a solution without linear regulators would improve this to 75%-80%.

Magnetic and Radiation Tolerance Criteria for COTS parts

		Inner Rim ($R = 1\,\mathrm{m}$)	Outer Rim ($R = 5\,\mathrm{m}$)
TID	(γ)	$1740\,\mathrm{Gy}$	$84\,\mathrm{Gy}$
NIEL	(fast neutrons)	$2.1 \times 10^{14}\,\mathrm{n/cm^2}$	$7.1 \times 10^{12}\,\mathrm{n/cm^2}$
SEE[1]	(protons)	$4.3 \times 10^{13}\,\mathrm{p/cm^2}$	$1.4 \times 10^{12}\,\mathrm{p/cm^2}$
B field		$\leq 1\,\mathrm{kG}$	$5\,\mathrm{kG}$

[1] Simulated number of hadrons with $E > 20\,\mathrm{MeV}$

Table 2: Radiation and magnetic tolerance criteria. Radiation numbers assume 10 years at an LHC luminosity of $\mathcal{L} = 5 \times 10^{34}\,\mathrm{p/cm^2 s}$. Safety factors include are appropriate for homogenous-batch COTS devices with control for dose-rate effects. A 30% increase can be expected from the JD shielding redesign.

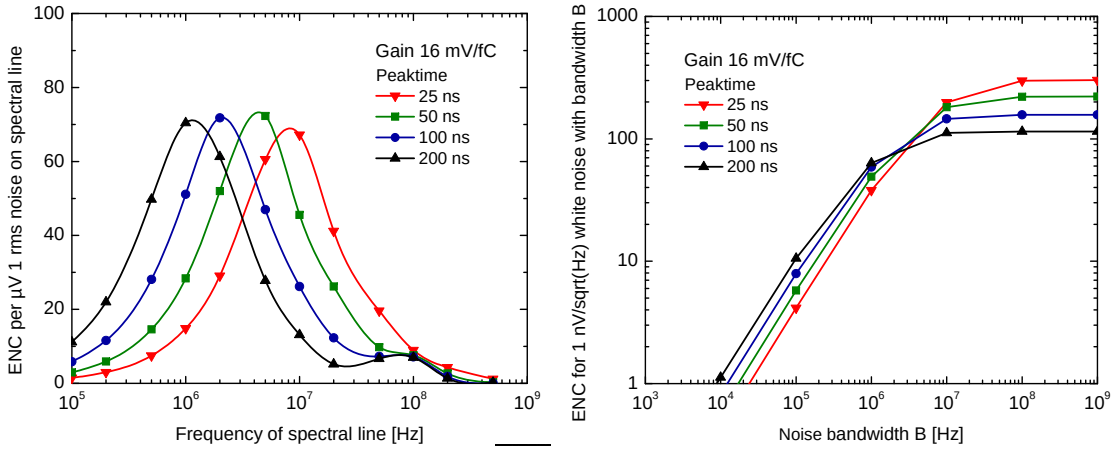

(a) (b)

Figure 1: The noise sensitivity of the VMM2 [1]. Figure (a) shows the noise in terms of equivalent noise charge per micro-volt RMS noise at a given frequency. Figure (b) shows this integrated over a white noise spectrum up to the specified cutoff frequency.

reason, we also consider the possibility of direct power from an extremely low-noise DC-DC converter.

The VMM has demanding noise requirements for its analog supply. Figure 1 shows the simulated sensitivity of the VMM2 to power supply noise. Figure (a) show the equivalent noise charge (ENC) induced per microvolt noise at the given frequency. Figure (b) shows the integral of the ENC assuming a white noise spectrum cutoff at a maximum frequency B. Ideally, the ENC would be kept to 100 electrons or less [1]. This indicates that at the megahertz-scale frequencies associated with compact DC-DC converters, the noise at the fundamental frequency should be of the order of $1\,\mu\mathrm{V}$.

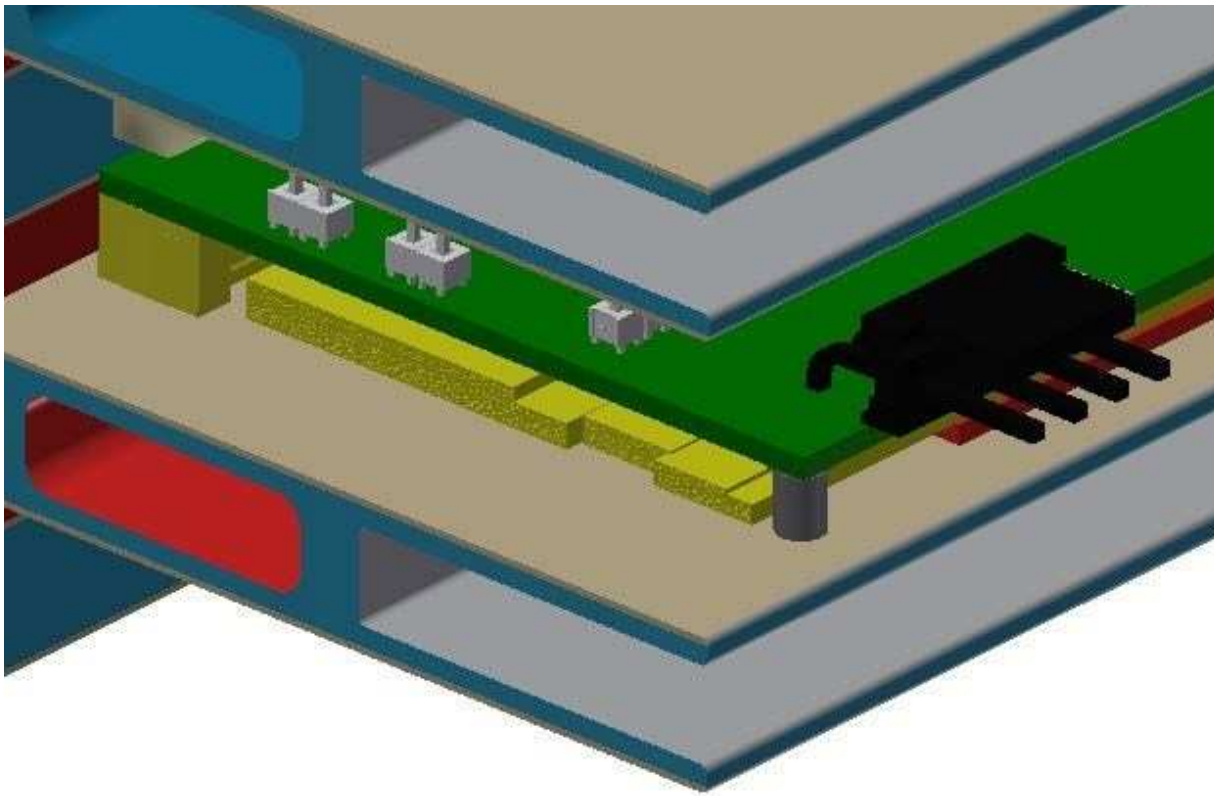

Figure 2: The edge of a single MicroMegas quadruplet. Shown are the two parallel cooling channels and the placement of an MMFE8 board. There is 6 mm between the component-side of an MMFE and its cooling channel. The distance between the reverse side and the next cooling channel is slightly over 13 mm.

2.3 MicroMegas Cabling, Cooling and Mechanical

The most stringent space constraints are associated with the MicroMegas front-end boards (MMFE). These boards are situated along the edges of each MM plane; each board hosts 8 VMM chips and supporting circuitry in order to provide digitization and readout of detector signals. Cooling channels, which also serve as cable raceways, are located between adjacent rows of MMFEs. This is shown in Figure 2.

The component-side of an MMFE faces its associated cooling channel, separated by a gap of approximately 6 mm. The exact value will depend on the final choice of attachment method for the MMFE. A machined cooling plate located in this gap will provide thermal contact between the heat-generating components and the channel. The reverse side of the board is less constrained; the boards located on the inner two planes will have some 13 mm between the reverse surface and the second cooling channel. If the final MMFE installation requires that the boards be inserted at an angle or offset from their final position, the effectively available height will be less.

The cooling scheme also constrains the LV power cabling to the FE boards. The open cavity in the cooling channel - 7 mm $\times$ 29.5 mm - is expected to house LV cabling, HV

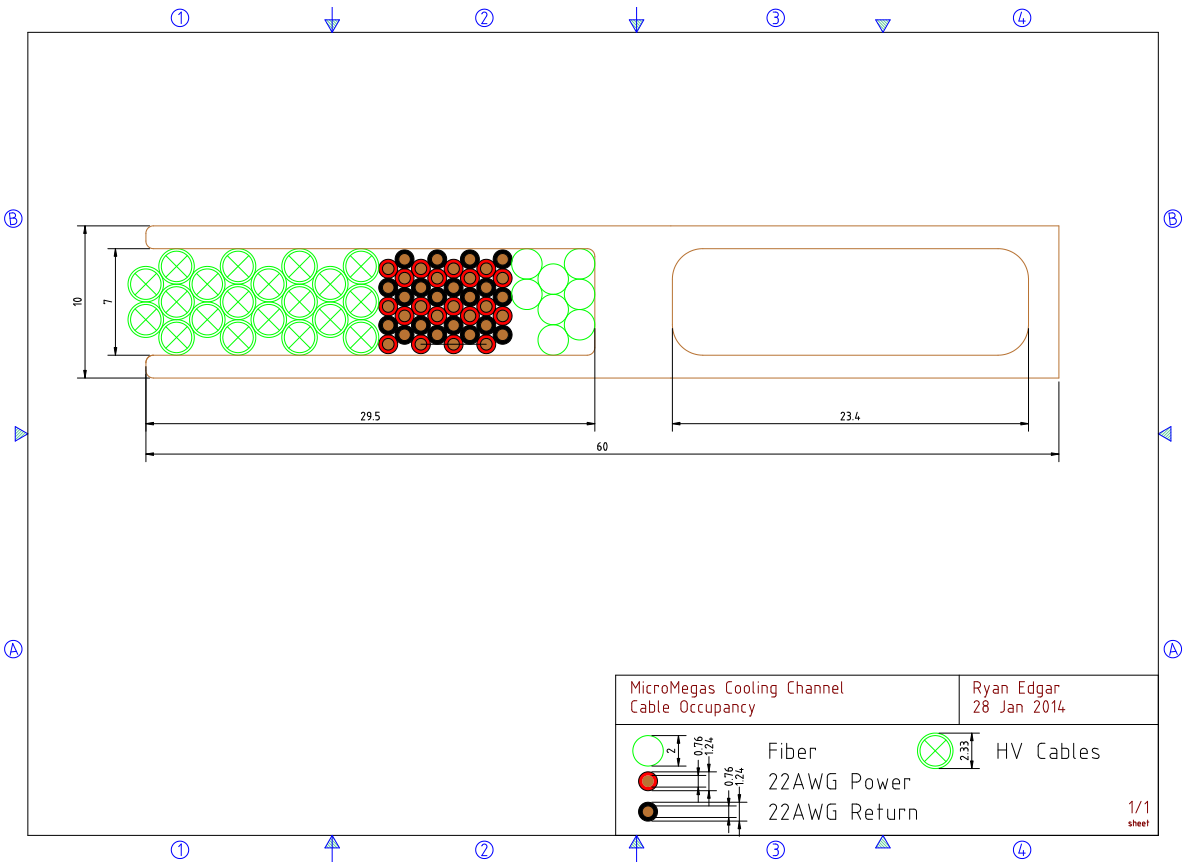

Figure 3: An illustration of the cabling occupancy of the MicroMegas cooling channel. The closed cavity on the right carries the cooling water through the channel, while the open cavity on the left is used as a cableway. The drawing is representative of the end of the channel furthest from the beamline, where cabling ccupancy is maximal.

cabling, and fibers for readout. If the FE boards are to have individual LV connections (ie. a star distribution topology), then after accounting for HV and fibers, the remaining space allows for 22AWG cables (Fig. 3). The longest cable runs (4 m) would have a resistance of 212 mΩ. This can supply a current of 1 A at 12 V at 95% efficiency (e.g. a 10 W MMFE8), which is sufficient in all scenarios for any of the FE boards that will be cabled through the cooling channel.

Constraints on the board surface area available for power are less easily quantified. However, the MMFE will be extremely densely populated, and any reduction of the power conversion area will help ease placement on and layout of the final board. As a point of reference, roughly 1600 mm^2-1700 mm^2 is used for power conversion and regulation on the MMFE8 demonstrator. This area contains four DC-DC converters and twelve LDOs.

3 On-FEB Power Conversion Options

3.1 COTS Buck Converters, LDOs

Compact buck converters providing 1 V-2 V from greater than 12 V input are widely used in consumer electronics and automotive applications. Low-dropout regulators are ubiquitous. Because the radiation loads in the New Small Wheel are relatively modest, this allows the possibility that commercial-off-the-shelf (COTS) power conversion devices may be suitable.

One advantage of this approach is cost, as COTS parts tend to be relatively inexpensive. A second and more important advantage is that the extensive commercial market for power conversion devices has produced a large collection of optimized solutions; many have desirable features that would ease board design and integration issues. A list of candidate devices was identified by a combination of market survey and recommendation (Table 3). The selected candidate parts include such features as multiple outputs (LTM4619, LTM4628, ADP5052), low radiated noise (LTM8033), or integrated magnetics (LTM8033, LTM4619, LTM4628).

3.2 FEAST

Point-of-load conversion is an attractive solution for many particle physics applications. In recognition of the common constraints in these applications, an extensive research and development effort in the CERN microelectronics group has undertaken to produce a common solution. The product of this effort, the FEASTMP [2, 3], is a 4 A-capable synchronous buck converter intended to provide POL regulation from a 5 V-12 V input. The FEAST ASIC is designed to withstand a total ionizing dose of 2×10^9 Gy and an integrated particle fluence of above 5×10^{14} n/cm^2 (1MeV-eq). The device is resilient against single-event effects and capable of operating in magnetic fields in excess of 40 kG.

The FEAST is normally provided as a mezzanine module with a stack height of 14.37 mm (Fig. 4). Much of the height is a result of the toroidal air-core power inductor, a necessity for operation in magnetic fields of tens of kiloGauss. The module's connector also contributes substantially to the height. Additionally, the module requires cooling via a pad located on the bottom of the module.

A lower-profile module, the FEASTMP-CLP, also exists. This module locates the connector on the opposite side of the board to reduce the stack height to 9.4 mm. This is a combination of 8.4 mm module height and a 1 mm mandatory gap between the module and the host board. Cooling is similarly accomplished through a thermal pad on the bottom of the module.

3.3 TPS7H1101: TI Space-Qualified LDO

A recent development is the beginning of discussions with Texas Instruments regarding a CERN bulk purchase of the TPS7H1101, a TI low-dropout regulator intended for space applications. This part is nominally available at 200USD in unit quantities. However, TI

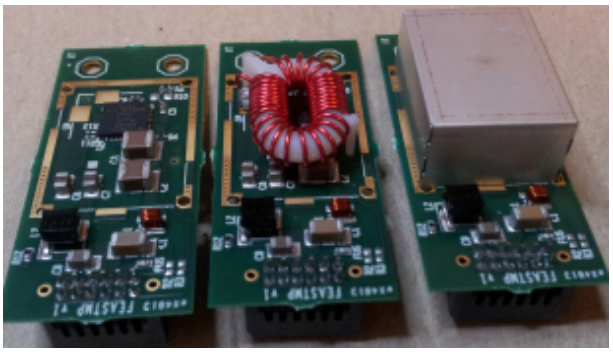

(a)

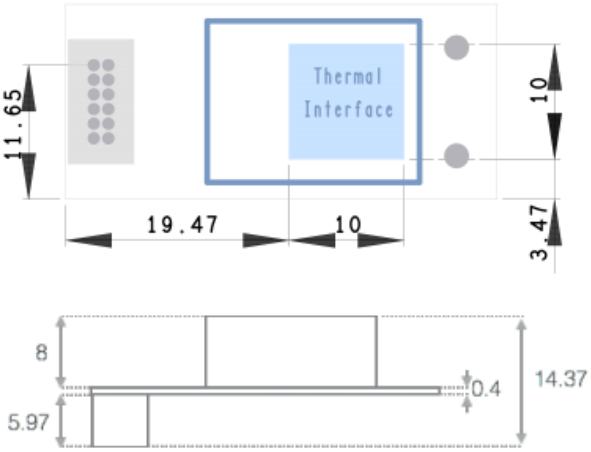

(b)

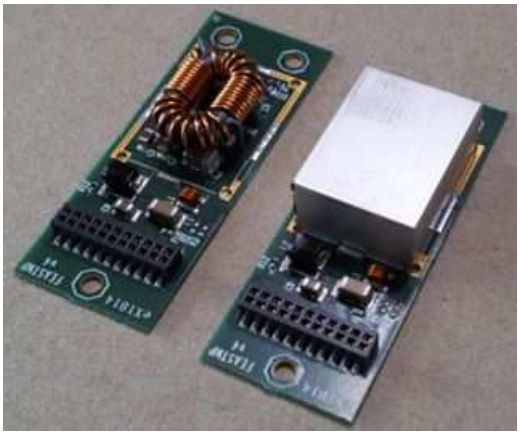

(c)

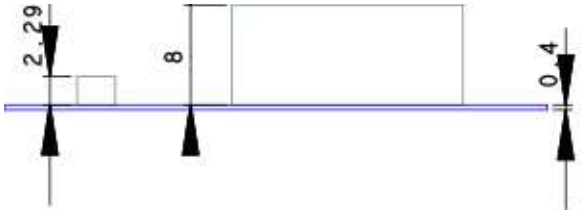

(d)

Figure 4: The FEASTMP module. Figure (a) shows the full module, with shield removed, and with air-core inductor removed. Figure (b) shows the module's dimensions. Figures (c) and (d) show the same for the lower-profile FEASTMP-CLP.

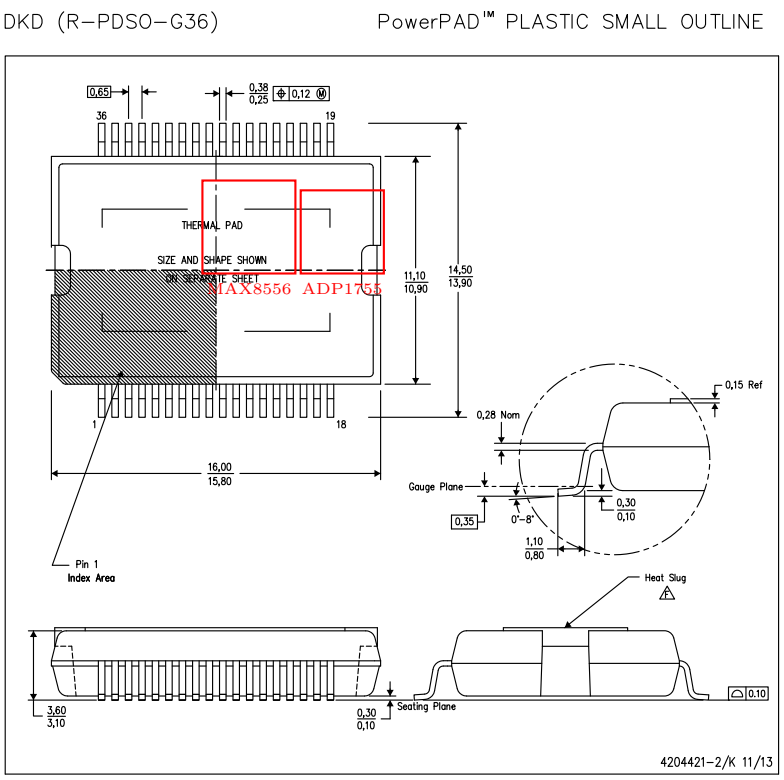

Figure 5: The physical specifications of one proposed package for the TI TPS7H1101. Shown for comparison are two COTS regulators, the ADP1755 and MAX8556.

has indicated that with less costly alternate packaging and a sufficiently large order, the part might be available for as low as 20-30USD per device.

This device is radiation-hard, although it has not yet been tested to the levels required in the New Small Wheel. TI has agreed to test the device's TID tolerance internally, and has also provided samples so that the device's tolerance to displacement damage may be evaluated as well. These tests are presently pending, but are likely to be successful.

Unfortunately, the TPS7H1101 die is physically large, which limits the available packages. One proposed package is shown in Figure 5, along with two candidate COTS regulators. It is unlikely that the size will be reduced much from this proposed package. Along with considerations of cost, this will likely mandate a minimal usage of LDOs should this device be a recommended options.

Manufacturer	Part	Nominal V_{in}		Outputs	Unit Cost
		12V	24V	Qty@I_{out}	(USD) ⋆
Linear Technology	LTM4619		×	2@4.0A	20.34
Linear Technology	LT8610		×	1@2.5A	4.31
Linear Technology	LTM4628		×	2@8.0A	24.16
Linear Technology	LTM8033		×	1@3.0A	14.51
Linear Technology	LTC3608	×		1@5.0A	9.11
Analog Devices	ADP5052	×		2@4.0A	4.31
				2@1.2A	
Analog Devices	ADP1864	×		1@5.0A	1.80
Texas Instruments	TPS53319	×		1@14.0A	3.62
ST Microelectronics	ST1S41	×		1@4.0A	1.07
CERN Microelectronics	FEAST2	×		1@4.0A	20.00

(a)

Manufacturer	Part	Current	Dropout[1]	PSRR[2]	Unit Cost
		(A)	(mV)	(dB)	(USD) ⋆
Linear Technology	LT3080	1.1	350	20	2.33
Analog Devices	ADP1755	1.2	105	40	1.31
Maxim Integrated	MAX8556	4.0	100	25	2.71
Texas Instruments	TPS74201	1.5	55	45	2.25
Texas Instruments	TPS7H1101[3]	≥1.0[3]	62	25	TBD
ST Microelectronics	LHC4913	3.0	1000	?	14.35

[1] At rated current.

[2] At 1 MHz

[3] Rated current and cost are package-dependent. This is under discussion with TI.

(b)

Table 3: A comparison of the candidate devices. The majority are COTS devices. The FEAST is a radiation-hard part produced by CERN microelectronics. The TI TPS7H1101 is a space-qualified commercial part. Table (a) shows DC-DC converters and (b) shows low-dropout regulators.

Part	Rate (Gy $h^{-}1$)	Dose at Failure (Gray)
Candidate Buck Converters		
LTM8033	5	≥ 4000[1,2]
LT8610	10	≥ 4000[2]
LT8610	16	3300[3]
LTM4628	16	1540[3]
ADP5052	16	750[3]
ADP1864	16	630[3]
TPS53319	16	260[3]
ST1S41	16	240[3]
LTM4619	5	≥ 4000[2]
LTM4619	16	2000[3]
LTM4619	22	2300[2]
LTM4619	22	1800[2]
LTM4619	50	300[3]
MAX8556	1500	2400[4,5]
ADP1755	1500	2300[4]
LT8612	1500	400[4]
Candidate Low-Dropout Regulators		
TPS74401	16	910[3]
LTM3083	16	900[3]

[1] Deviations of above 20% in V_{out} observed during testing.
[2] ENEA Calliope.
[3] Brookhaven SSIF.
[4] High-rate TID data inferred from proton exposures (subsequent section).
[5] Device later regained functionality after annealing at room-temperatures.

Table 4: The dose of ionizing radiation at which failure was observed during ^{60}Co exposures. The results are arranged in descending order by dose rate. The LTM4619 is displayed separately to illustrate the enhanced tolerance to ionizing radiation that is evident at lower rates. This table also includes TID tolerance data obtained from proton testing. The extremely high dose rate likely reduces the measured TID tolerance compared to the low-rate ^{60}Co exposures.

4 COTS Radiation and Magnetic Field Testing

5 Ionizing Radiation (TID)

Although the total dose in the operating environment is large, it is accumulated over the New Small Wheel's ten-year design lifetime at a rate of only $20\,\text{mGy}\,\text{h}^{-1}$. Because many modern semiconductor technologies are known to exhibit some degree of annealing at room temperature, the failure-dosages measured at high rates may not accurately reflect the failure-dosage in the low-rate environment of the New Small Wheel. To minimize this effect, candidate devices were irradiated over the longest possible times.

Exposures were conducted at two ^{60}Co sources: the Solid State Irradiation Facility (SSIF), a $4 \times 10^{13}\,\text{Bq}$ source operated by Brookhaven National Laboratory in the United

States; and Calliope, a 3×10^{15} Bq source operated by ENEA Casaccia in Italy. Buck converters were powered by 24 V during irradiation, while providing 1.5 V to either resistive loads or voltage regulators on their outputs. Voltage regulators in turn were supplied by 1.5 V while providing 1.2 V to resistive loads. Input voltage, input current, and output voltage for each device were monitored for the entirety of each exposure.

Several irradiation campaigns were conducted at these facilities, ranging in duration from 1-40 days at rates between 5 Gy h^{-1} and 22 Gy h^{-1}. The dosages at failure from these and other tests are summarized in Table 4. One part, the LTM4619, has been tested at a particularly large variety of dose rates, and the tolerance to ionizing radiation is seen to improve markedly as the dose rate decreases. The LT8610 appears to be affected similarly, though here there are fewer data points.

6 Displacement Damage (NIEL)

Those parts that appeared to display sufficient tolerance to ionizing radiation were subsequently tested for susceptibility to displacement damage using fast neutrons. An initial exposure was conducted at the Fast Neutron Irradiation Facility (FNI), operated by the University of Massachusettes, Lowell. An unpowered collection of modules that included the LTM8033, LTM4628 and LT8610 were exposed to a total fluence of 1×10^{13} n/cm^2 1 MeV (Si). The LTM4628 experienced a small (<10 mV) increase in output voltage. The output voltage of the LTM8033 was shifted by 40%, from 1.5 V to 2.1 V. No observable changes occurred in the LT8610.

A second exposure at FNI was conducted to a higher fluence with the samples powered. The two-hour exposure reached 5×10^{14} n/cm^2 1 MeV (Si) equivalent neutrons. Twelve devices in total were irradiated: six LT8610, one LTM4628 and one LTM4619, along with four voltage regulators. The devices were placed into a sealed aluminum cell and lowered 6 m into the reactor water. Power and monitoring were supplied remotely from the surface through sealed, watertight cable assemblies. The parts were provided with in-situ resistive loads as above.

At a total fluence of 2.5×10^{14} n/cm^2 1 MeV (Si), the LTM4619 experienced abrupt failure. One voltage regulator, the LT3080, experienced failure at a fluence of 5×10^{13} n/cm^2 1 MeV (Si). The remaining modules survived the testing. The LT8610 and LTM4628 displayed output voltage shifts of 30 mV-50 mV, which is likely a result of accumulated damage to internal voltage references.

Finally, the modules that had been previously exposed to gamma radiation at Calliope were subsequently exposed to neutrons at TAPIRO, a 5 kW research reactor with dry irradiation channels operated by ENEA Casaccia. This exposure was conducted with devices under power to a total fluence of 1×10^{13} n/cm^2 1 MeV (Si). The LTM8033 remained operational through the test, but the output voltage shifted upward by 50%. The LTM4619 failed completely after 8×10^{12} n/cm^2, while the LT8610 was entirely unaffected. The failure of the LTM4619 is likely due to additional ionizing radiation accumulated during the fast neutron exposure. These results are summarized in Table 5.

Part	Dose at Failure (10^{14} n/cm^2)	
Candidate Buck Converters		
LT8610 (x6)	≥ 5.0 [1]	
LT8610	≥ 0.1 [2]	Device previously exposed to 4 kGy
LTM4628	≥ 5.0 [1]	
LTM8033	0.1 [2]	Output voltage shift of 50%
LTM4619	2.6 [1]	
LTM4619	0.08[2]	Device previously exposed to 4 kGy
Candidate Low-Dropout Regulators		
LT3080	0.5 [1]	
ADP1755	3.3 [1]	
TPS74201	3.8 [1]	

[1] UMass Lowell FNI
[2] ENEA-Casaccia TAPIRO

Table 5: Dosages at failure for devices irradiated with fast neutrons.

6.1 Single Event Effects

Power conversion devices that contain digital circuitry - such as soft-start or reset flip-flops - can be vulnerable to single-event effects from highly ionizing particles. In the radiation environment of ATLAS, this occurs primarily through nuclear recoil: a incident hadron striking a nucleus in the device itself produces an energetic heavy ion, which in turn deposits large amounts of charge in a localized area.

To test for single-event effects, devices were irradiated with proton at energies up to 220 MeV at the CDH Proton Center in Warrenville, Illinois. The devices were exposed to fluxes from 1×10^8 p/cm^{2}s-4×10^8 p/cm^{2}s until a total fluence of 5×10^{12} p/cm^2 was reached or until device failure. In addition to the desired nuclear recoils, this proton flux also deposits ionization at rates of up to several thousands of grays per hour. As such, TID-induced failure is expected during the course of exposure.

Proton irradiations were conducted on the most promising remaining devices: the LTM4619 buck converters, and ADP1755 and MAX8556 voltage regulators. Also included was the LT8612, a newly-released product produced using the same process as the LT8610 but with greater current capability. The devices were exposed under power, with resistive loads, and with input and output voltage monitored by a triggered data acquisition system. Rising or falling edges that exceeded a window of $\pm 15\%$ around the nominal output voltage initiated acquisition. This captured an inverval that spanned from 10 ms before the triggering event to 65 ms after.

All tested devices displayed some sensitivity to single-event effects; some examples are shown in Figure 6. The observed events range in their potential impact to downstream electronics. The least problematic are short proton-induced resets, e.g. (c) and (e). These have a time scale of some 50 µs-100 µs, which is short enough to be ameliorated with sufficient capacitive filtering. More problematic are long proton-induced reset and oscillation events, such as (a), (d), and (f). These last for tens of milliseconds, which is too long to easily filter and could result in the loss of volatile data in downstream

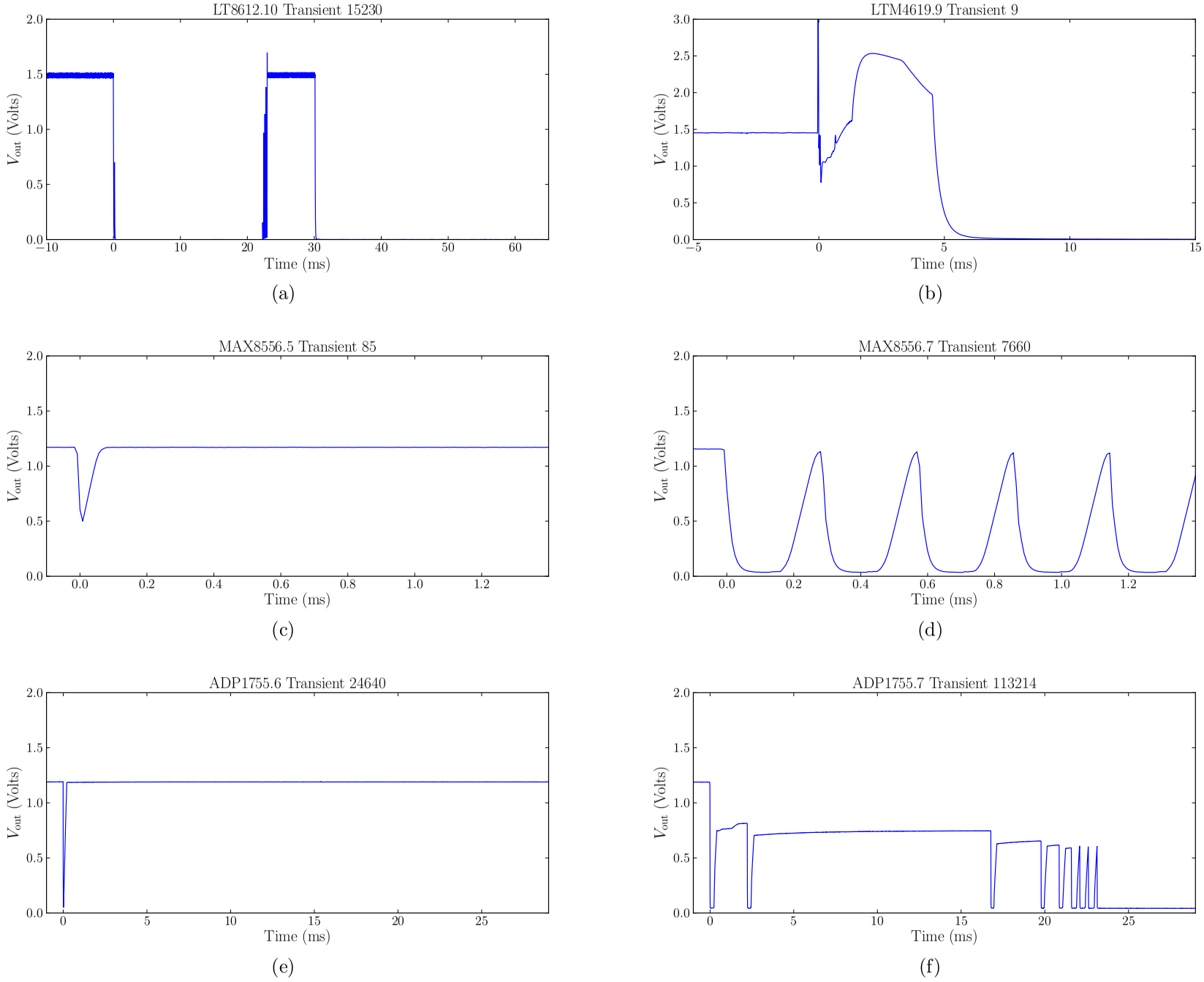

Figure 6: Examples of single-event effects observed in 220 MeV protons. Figure (a) shows two proton-induced resets in an LT8612 occuring in rapid succession. Figure (b) shown a suspected destructive single-event effect in an LTM4619. Figures (c) and (d) show proton-induced resets and oscillations in the MAX8556. Figures (e) and (f) show similar events for the ADP1755.

Device	Proton Energy (MeV)	Cross-Section 10^{-12}cm^{-2}	Notes
ADP1755	220	277 ± 8	Short transients
	220	83 ± 4	Long transients
MAX8556	≥40[1]	71 ± 4	Short transients
	≥40[1]	0.50± 0.35	Long oscillations[3]
LTM4619	220	6[2]	Destructive
LT8612	220	680 ±50	Multi-millisecond drops
MAX8556	220	2 ± 1	Long oscillations[3]
MAX8556	220	83 ± 8	Short transients
MAX8556	170	64 ± 9	Short transients
MAX8556	120	76 ± 9	Short transients
MAX8556	70	58 ±10	Short transients
MAX8556	40	58 ±10	Short transients
MAX8556	20	13 ± 3	Short transients

[1] Combined result from individual measurements in the second part of the table.
[2] One event; no error is assigned.
[3] These were observed only at 220 MeV, and not in lower-energy exposures.

Table 6: Measured single-event cross-sections for buck converters and voltage regulators irradiated in a proton beam.

electronics (e.g. configuration registers). Most troubling is (b), which appears to be a destructive single-event effect in an LTM4619.

The measured cross-sections for these devices are shown in Table 6. As a point of reference, at a distance of 1 m from the interaction point, a cross-section of $7.3 \times 10^{-14}\,\mathrm{cm}^{-2}$ is equivalent to one SEE per device per year and a cross-section of $2.7 \times 10^{-11}\,\mathrm{cm}^{-2}$ equivalent to one SEE per device per day. At these levels, only the MAX8556 appears to be usable in all regions of the NSW. The observation of destructive single-event effects in the LTM4619 entirely preclude its use. The LT8612's large cross-section would result in several resets per day for devices located at $r = 1\,\mathrm{m}$.

6.2 Magnetic Field Tolerance

Several of the candidate parts are packaged modules that include integrated magnetics (LTM8033, LTM4619, LTM4628). This is desirable from the standpoint of system integration, as it reduces the parts count and the footprint for the power circuitry while at the same time simplifying the design of the front-end boards. However, the 0.3 T-0.6 T magnetic fields in the New Small Wheel are large enough to potentially saturate magnetic materials.

These modules were tested for their ability to tolerate these magnetic fields at a 1 T conventional electromagnet housed at the Laboratorio Acceleratori e Superconduttiviatà Applicata, operated by INFN and the University of Milan (see also Ref. [4, 5]). Two LTM8033 and one LTM4619 were exposed to magnetic fields in three different orientations (Figure 7). The LTM8033, which includes additional magnetic shielding to suppress RF interference, was able to operate in fields as high as 1 T with only small reductions in

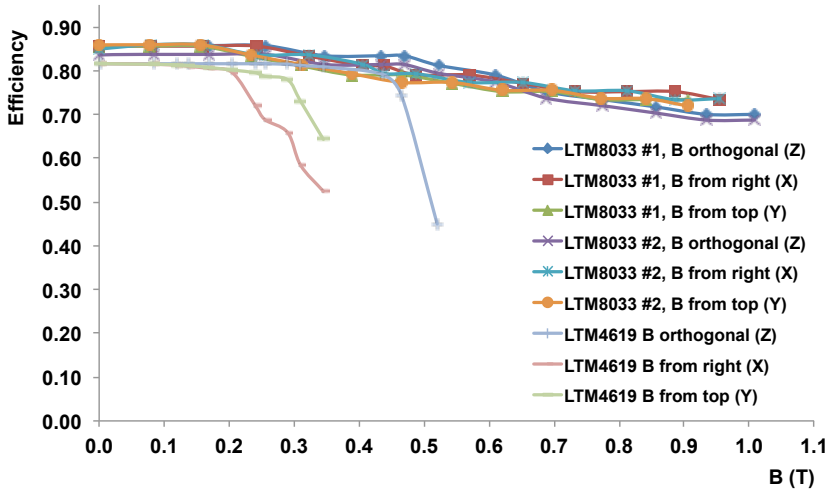

Figure 7: The efficiency of the LTM8033 and LTM4619 packaged modules as a function of magnetic field strength. These modules include integrated magnetics, and therefore may be affected by external magnetic fields.

efficiency. The LTM4619 tolerated fields as high as 0.5 T when the field was perpendicular to the plane of the board, but was only able to function to 0.3 T with the field parallel.

6.3 Summary

Table 7 displays the most limiting known tolerance for each of the tested commercial devices. Although several COTS parts appeared promising in test of TID and NIEL tolerance, subsequent tests for single-event effects in protons have uncovered several troubling behaviors. This suggests against the use of these devices on electronics that will be located near the inner radius of the NSW. The potential exception is the Maxim MAX8556, however, this part requires additional testing to demonstrate its tolerance to displacement damage.

Although most of the COTS devices cannot be recommended for use in the high-radiation inner radii, the potential remains that some may be of use in the lower-radiation region on the outer edge of the New Small Wheel. The large magnetic field there precludes the use of the devices with integrated inductors. However, the Linear Technology LT8612 is likely viable in this region, particularly if measures such as multiply-redundant devices are taken to mitigate the single-event resets.

7 COTS Inductors

Although some of the candidate DC-DC converters include integrated magnetics, most require external power inductors. In addition, smaller inductors will be used extensively for filtering. In many cases this could be done with air-core inductors, however, the space saved by more compact ferrites is of value on the densely-populated front-end boards.

Test Notes

Part	Limiting Tolerance	
Candidate Buck Converters		
LTM4619	B	3 kG
	SEE	destructive
LT8610	I_{out}	2 A
LT8612	SEE	$\sigma_S E = 6.8 \times 10^{-10}\,\text{cm}^{-2}$
LTM4628	B	3 kG
LTM8033	NIEL	10^{13} n/cm^2
LTC3608	NIEL	10^{13} n/cm^2
ADP5052	TID	750 Gy
ADP1864	TID	630 Gy
TPS53319	TID	260 Gy
ST1S41	TID	240 Gy
Candidate Low-Dropout Regulators		
LT3080	NIEL	5×10^{13} n/cm^2
ADP1755	SEE	
MAX8556	viable?	
TPS74201	engineering (V_{bias})	

Neutron dosages in 1 MeV (Si) equivalent.

Table 7: A summary of the limiting tolerances of the devices of interest. In all cases except the MAX8556, expected radiation doses near the inner rim of the NSW exceed these tolerances. Some devices (e.g. the LT8612) appear suitable for usage on the outer rim.

Ferrite inductors, however, suffer from a loss of inductance when subject to external magnetic fields.

A testing program was conducted to locate ferrite-cored inductors, both for power and for filtering, that are sufficiently tolerant of magnetic fields for use in the New Small Wheel. The results are shown in Table 9. Numerous inductors from several manufacturers were tested in a Neodymium-Iron-Boron magnet fixture able to produce fields up to 6.5 kG. The performance of the inductors was characterized by measuring their inductance as a function of the external field strength. Molded inductors, in which the coil is sintered into a block of powdered iron, were typically the best performers. While most other inductor geometries fall to 5-20% of their initial inductance in a 6.5 kG field, several molded inductors were found that retain nearly 50% of their inductance at these field strengths.

8 Adapting the FEAST

The mechanical constraints of the FEASTMP and FEASMP-CLP modules are challenging. While the latter can meet the height constraints for the MMFE, the module's requirements that cooling be provided from the bottom pad does not readily integrate with the MicroMega's cooling system. Additionally, the 1 mm space between the module and FEB produces dead space on the FEB, where component placement becomes difficult or

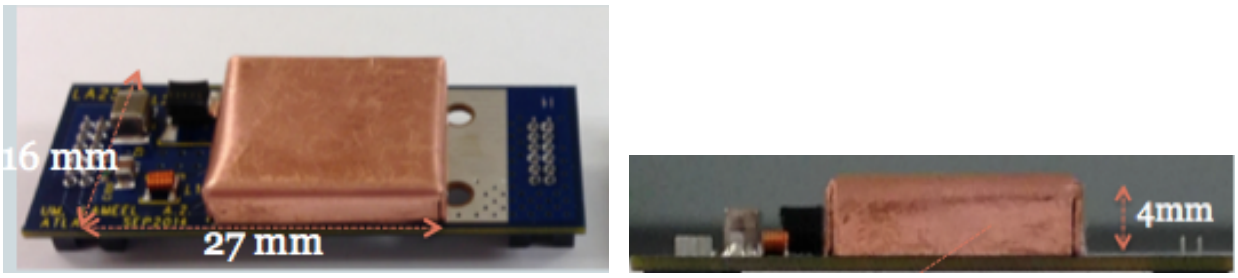

(a) (b)

Figure 8: A prototype ultra-low-profile FEAST-based DC-DC converter. The protype was constructed as a module compatible with the original FEAST for convenient testing. The shield was constructed from heavy-gauge copper to allow the shield to serve as an alternate cooling path. The area required when integrated on a PCB is 16 mm × 27 mm. The height is 4 mm, but could be reduced further.

impossible.

One option to address these constraints is to integrate the FEAST directly on the FEBs using low-profile B-tolerant ferrite inductors. This avoids the small but noticable voltage drop from the connector, minimizes the total height, and allows for the possible use of alternate cooling paths. To explore this usage of the FEAST ASIC, an ultra-low-profile module was constructed (Fig. 8). The design was produced as a module, and shares the same footprint as the original FEAST module for convenience in testing.

This implementation uses a surface-mount ferrite inductor identified during previous tests as being able to withstand magnetic fields as high as 6.5 kG. Integrated onto the front-end boards, the required area per converter would be 430 mm^2. The total height is only 4 mm, and with alternate choices of power inductor could be reduced to below 3 mm. Like the full-height FEAST module, a copper shield is included to reduce radiated emissions.

8.1 Electrical Performance

The regulation, efficiency, and noise of the module were characterized on the benchtop while providing 1.5 V output from a 10 V input voltage.

The regulation is shown in Figure 9a as the difference between the output voltage at the given current and the output voltage with no load. Curves are shown as measured on the load side of the connector (representative of use as a module) and as measured on the module itself (representative of direct integration on to a FEB). The difference seen between these two measurements is due to the series resistance of the module's connector. A corresponding plot of the efficiency is shown in Figure 9b. Here, the slightly lower resistance of the surface-mount ferrite as compared to the air-core toroid produces a slight increase in efficiency.

Extensive study was also performed by the FEAST designers to reduce the conducted noise on the converter's input and output [6, 7]. That work has been heavily drawn on here. The module's conducted noise was measured at load currents up to 4 A. Some noise

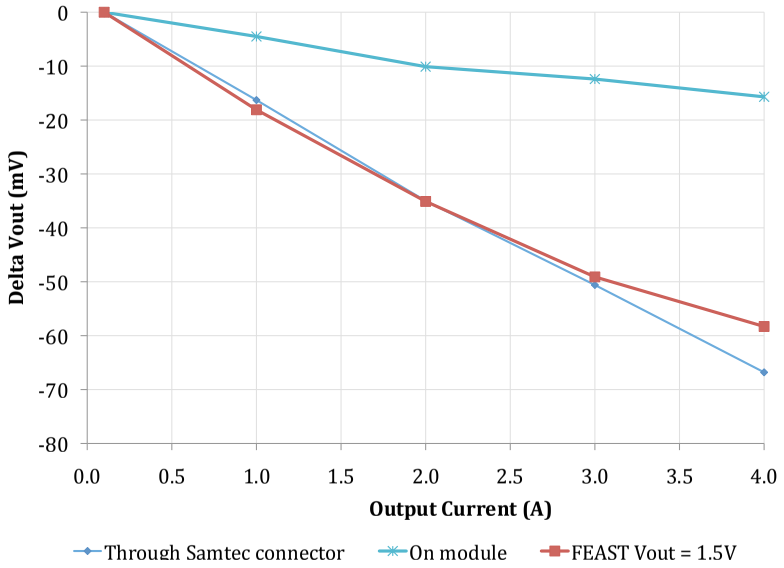

(a)

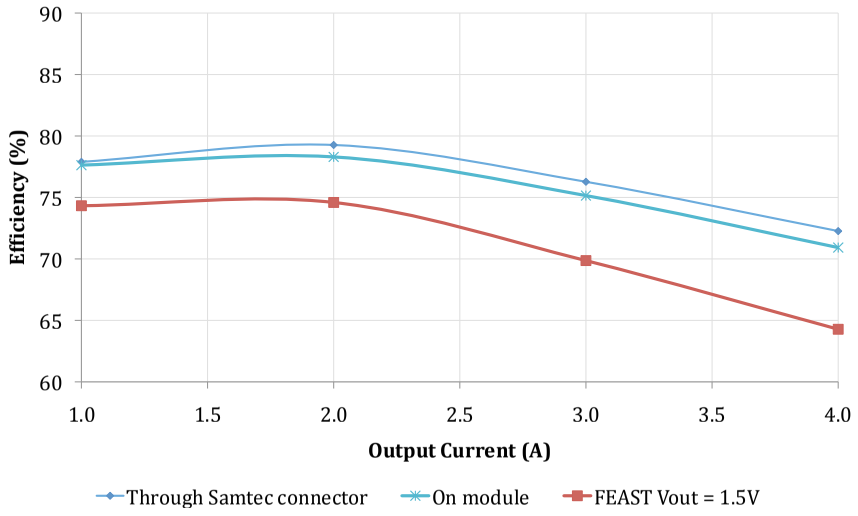

(b)

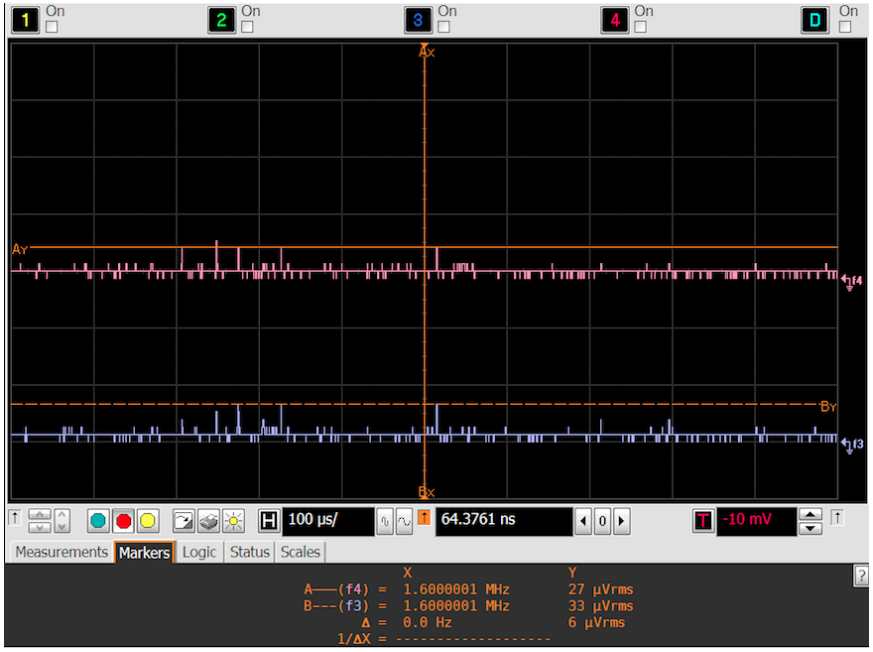

(c)

(d)

Figure 9: Regulation (a), efficiency (b), and conducted noise measurements of the ultra-low-profile FEAST module (blue curves). As a comparison, the full-height FEAST module with air-core toroid is also shown (red curve). Conducted noise is shown at load currents of 1 A (c) and 2 A (d). Note that the peaks below the 1.63 MHz ripple frequency are noise from the test environment.

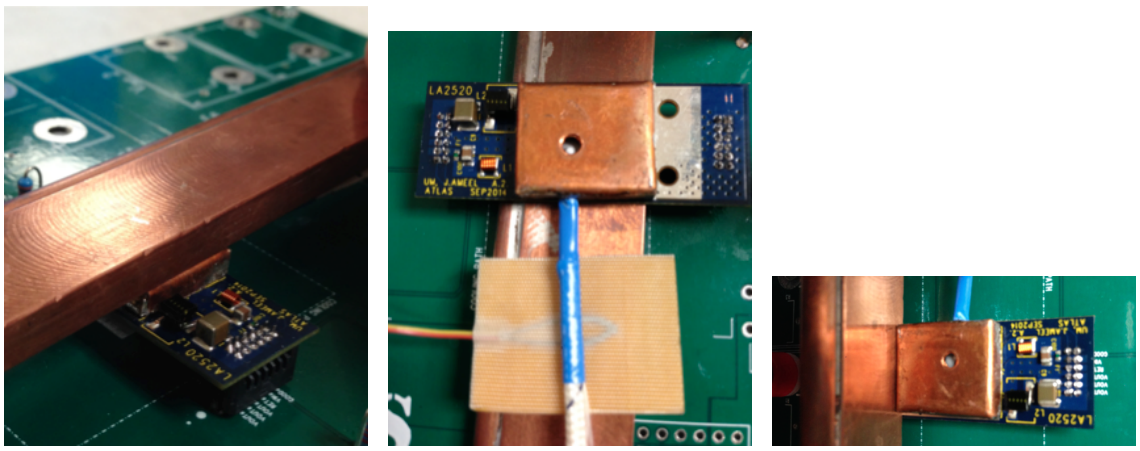

(a) (b) (c)

Figure 10: Tles.

results from the prototype module are shown in Figures 9c and 9d, with the converter providing 1 A and 2 A respectively. The latter was the noisiest case observed over the full output current range, with an amplitude of 40 µV on the output at the converter's 1.63 MHz switching frequency. Although in isolation this does not yet meet the demanding VMM noise requirements, it was achieved with relatively modest component values. Larger filter components or the addition of another filtering stage can readily reduce it much further.

8.2 Cooling

To evaluate different cooling strategies, the ultra-low-profile FEAST included multiple cooling paths: a cooling pad located underneath the test board (Fig. 10b), a copper finger on top of the test board (Fig. 10c), and the shield (Fig. 10a), which was designed to double as a heat-transfer mechanism.

The cooling paths were characterized by measuring the thermal resistance between the ASIC case and a heatsink in good thermal contact (a copper bar). The case thermocouple was attached with thermal epoxy to ensure good thermal contact. This method is imperfect, but provides a useful comparison. At present, methods are being investigated to measure the die temperature directly.

The results of these measurements are shown in Table 8. A corresponding measurement of the full-height FEAST provides a point of comparison. Additionally, the measurements were repeated after filling the shield completely with thermal grease. In both cases the underside cooling pad is the most effective solution. However, the injection of thermal grease improved the heat transfer performance markedly, and can allow adequate cooling through the shield.

Cooling Paths	Thermal Resistance (°C/W)	
	Air	Thermal Grease
Underside	7.8	3.9
Shield	14.4	5.1
Cooling Finger	19.6	10.8
Underside (FEAST)	5.3	

Table 8: Measured thermal resistances between the ASIC case and heatsink for the ultra-low-profile FEAST. Measurements are shown with and without the shield filled with thermal grease. The full-height FEAST is included (final line) with the same measurement methodology as a point of comparison.

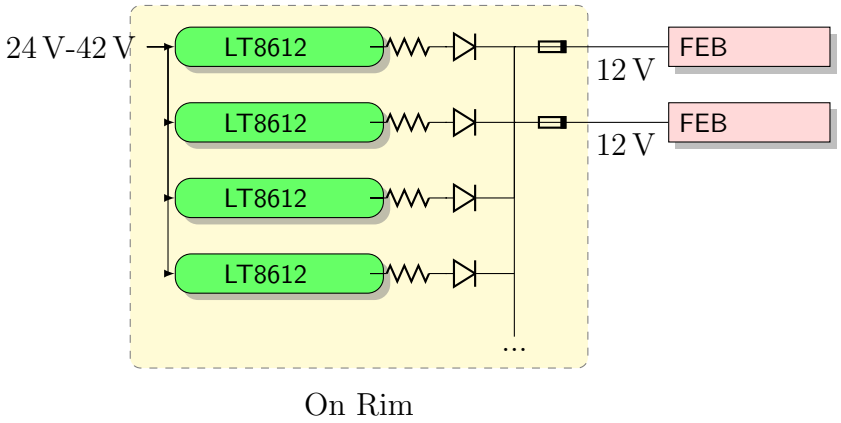

Figure 11: Conceptual diagram of an LT8612-based solution for conversion on the rim. Multiple LT8612s are paralleled through diodes to provide sufficient current for a single MicroMegas layer. This could be implemented with $N+1$ or $N+2$ redundancy to provide resilience against single-event effects and premature failure of any one converter.

8.3 Intermediate Conversion Stage

The usage of FEAST-based converters for the MicroMegas front-end electronics limits the delivery voltage at the FEBs to 12 V. While the cabling is achievable between the rim and the FEBs (see Sec. 2.3), service constraints require that power be delivered to the rim at at least 24 V. This requires an additional conversion step from 24 V to 12 V. The implementation of this conversion step is a critical reliaility issue, as the failure of a conversion stage that powers multiple downstream components will render all of those components inoperable. One advantage is that it provides a natural distribution point as well as a location for circuit protection and ballast resistors as per the NSW grounding guidelines.

This conversion step might be accomplished with a commercial product, although it is likely that such a product would either need to designed specifically for the NSW (or heavily adapted) in order to integrate into the mechanical environment. Another possibility is a custom implementation, and some of the COTS parts that are not suitable for the FEBs could be useful in this role instead. One possible solution, based on the

LT8612, is shown in Figure 11. The LT8612 can accept an input voltage of up to 42 V and produce an output current of 6 A at any lower voltage. Paralleling several converters using diodes can provide $N+1$ or $N+2$ redundancy, thus protecting against SEE and/or premature failure of any one converter. This would require N=4 if one supply handles a single MicroMegas layer, or N=2 for one side of one layer.

Note also that this conversion step, whether commercial or custom, need not be located on the rim; it could conceivably be placed along the MM cooling channels in an unused located to take advantage of the existing cooling system.

9 Status and recommendations

Of the buck converters that have been evaluated for use in the New Small Wheel, no COTS option appears fully viable in the higher-radiation regions at low radii. Both the leading COTS candidates - the LT8612 and LTM4619 - display troubling single-event effects when exposed to protons. The LTM4619 is strongly affected by magnetic field levels that would be present on the NSW rim. The LT8612 appears usable on the rim, e.g. as a conversion step to provide 10 V-12 V to electronics located in higher-radiation regions, particularly if measures are taken to mitigate the impact of single-event effects.

The FEAST, while not usable in it's module form, does not suffer from radiation concerns. Our recommendation is to integrate the FEAST ASIC(s) directly onto the front-end boards. This produces the best electrical performance while minimizing the required PCB area. With a magnetically-tolerant low-profile ferrite, the total height of this solution is 4 mm. This imposes minimal constraint on placement due to height. Cooling from either above or below is viable with this solution. Furthermore, the cooling channel capacity is adequate for cables supplying 10 V from the rim without undue cable loss.

This solution necessitates an additional conversion step on the rim. As mentioned above, the LT8612 appears suitable for this task. However, exploring the optimal means of accomplishing this conversion step remains an open issue.

Three possibilities presently remain for voltage regulators. The space-qualified Texas Instruments TPS7H1101 is being explored as an option, however, its large size and presently-unknown price may limit its application. One COTS regulators, the Maxim MAX8556, appears sufficiently resilient but still requires evaluation for its susceptibility to displacement damage. This is currently in progress. One final option is that voltage regulators may prove unnecessary - the conducted noise from the FEAST can be reduced to extremely low levels with only moderate passive filtering. This possibility would best be tested by integrating a FEAST-only power solution into a demonstrator front-end board and evaluating the effect.

In summary, the remaining open issues are:

1. Fully resolve the integration of the FEAST, along with noise and cooling issues, and produce a reference design for board designers.

2. Qualify the MAX8556 or TPS7H1101, or validate the no-voltage-regulator options.

3. Understand the options for conversion on the rim, commercial vs. custom with the LT8612, and from where it would be procured.

Table 9: Measured inductance for a variety of COTS parts in several magnetic field strengths.

Inductor Magnetic Field Tolerance

	Manufacturer	Part	Inductance Rated	B=0	B=2kG	B=4kG	B=6.5kG
		Power Inductors (Testing @ 1.8MHz)					
1	Coiltronics	HCM0703-R47-R	0.47	.58	.54	.42	.15
2	Coiltronics	HCM0703-1R0-R	1.00	.97	.88	.71	.36
3	Coiltronics	HCM0703-4R7-R	4.70	5.15	4.57	3.52	1.65
4	Coilcraft	XAL5030-601MEB	0.60	.69	.46	.40	.11
5	Coilcraft	XAL4020-601MEB	0.60	.57	.43	.33	.12
6	Coilcraft	XAL4020-102MEB	1.00	1.01	.65	.48	.19
7	Coilcraft	XAL5030-222MEB	2.20	2.11	1.31	.73	.31
8	Coilcraft	XAL5030-472MEB	4.70	5.57	3.07	1.61	.68
9	Coilcraft	XAL4030-472MEB	4.70	4.44	2.59	1.71	.61
10	Vishay-Dale	IHLP-2525CZERR47M01	0.47	.56	.42	.33	.15
11	Vishay-Dale	IHLP-2525CZ-01	1.00	1.07	.98	.84	.49
12	Vishay-Dale	IHLP-2525CZER4R7M01	4.70	3.75	3.41	2.75	1.24
13	Wurth	744 355 147	0.47	.42	.18	.16	.09
14	Wurth	744 373 460 047	0.47	.59	.53	.45	.14
15	Wurth	744 310 055	0.52	.60	.49	.43	.12
16	Wurth	744 778 004	0.52	.57	.09		-
17	Wurth	744 311 068	0.68	.72	.47	.39	.09
18	Wurth	744 778 001	1.00	.99	.12	.11	.10
19	Wurth	744 311 220	2.20	2.41	1.70	.72	.24
20	Wurth	744 778 002	2.20	2.31	.28	.27	.20
21	Wurth	744 373 460 33	3.30	3.27	2.90	2.32	1.06
22	Wurth	744 355 137 0	3.70	3.35	1.41	.56	.47
23	Wurth	744 373 240 47	4.70	4.97	4.50	3.33	1.90
24	Wurth	744 778 005	4.70	4.04	.53	.48	-
25	Wurth	744 311 220	6.50	6.55	3.35	1.08	-
26	Wurth	744 311 650	6.50	6.63	3.13	.96	.52
27	Wurth	744 373 461 00	10.00	10.30	10.10	8.56	6.52
28	Wurth	WE7447797470	4.70	4.32	.54	.52	.42
		EMI Chokes (Testing @ 1MHz)					
29	Fair-Rite	2744065447		2.72	.09	.08	-
30	Fair-Rite	2744045447		.88	.06	.05	-
31	Fair-Rite	2752041447		.16	.04	.04	-
32	Fair-Rite	2752045447		.40	.09	.09	-
33	Fair-Rite	2744555567		6.15	.07	.06	-
34	Fair-Rite	2744555577		10.46	.12	.10	-
35	Fair-Rite	2773021447		3.49	.05	.05	-
36	Fair-Rite	2773019447		1.80	.03	.03	-
37	Murata	BLM21PG221SN1D		1.54	.05	-	-
38	Coiltronics	MPI2520R0-R47-R	0.47	.60	.50	.35	.18

Continued on next page

Table 9 – continued from previous page

	Manufacturer	Part	Inductance Rated	B=0	B=2kG	B=4kG	B=6.5kG
39	Coiltronics	MPI2520R1-R47-R	0.47	.43	.34	.17	.11
40	Bourns	SRR0603-100ML	10.00	9.71	1.48	1.33	1.19
41	Vishay-Dale	ILHB0603ER600V		.40	.02	.02	.01
42	Vishay-Dale	ILHB0603ER121V		.91	.06	.05	.04
43	Vishay-Dale	ILC0603ERR27J	0.27	.39	.39	.40	.40
44	Vishay-Dale	IMC0603ER15NG01	0.015				
45	Vishay-Dale	IMC0603ER22NG01	0.022				
46	Vishay-Dale	IMC0603ER3N3S	0.0033				
47	Vishay-Dale	IMC0603ER15NG	0.015				
48	Coilcraft	1206USB-172MLB		1.74	.09	.06	
49	Coilcraft	1206USB-371MLB		.42	.07	.06	.06
50	Coilcraft	1206USB-102MLB		.51	.09	.06	.04
51	Wurth	782 633 620		.50	.04	.02	
52	Wurth	782 631 101		.23	.07	.06	.05
53	Wurth	782 633 601		4.58	.14	.09	.08
54	Yuden	BRC1608TR77M	0.77	.75	.30	.12	.12
WE Inductor Testing MAPI and LHMI Families(Testing @ 1MHz)							
55	Wurth	744 373 240 10	1	1.03	.95	.74	.43
56	Wurth	744 373 340 10	1	.94	.87	.66	.51
57	Wurth	744 373 460 10	1	1.05	.89	.59	.35
58	Wurth	744 383 130 033	0.33	.52	.45	.37	.26
59	Wurth	744 383 130 068	0.68	.76	.74	.59	.37
60	Wurth	744 383 130 10	1	.90	.85	.69	.48
61	Wurth	744 383 210 10	1	1.13	1.08	.89	.79
62	Wurth	744 383 240 10	1	1.09	1.03	.63	.42
63	Wurth	744 383 430 10	1	1.01	.96	.80	.52

References

[1] Gianluigi De Geronimo *Personal Communication*

[2] Michelis, S. *et al*, *DC-DC converters in 0.35μm CMOS technology JINST* **7 C01072**

[3] Abbate, C. *et al*, *Developments on DC/DC converters for the LHC experiment upgrades*, *JINST* **9 C02017**

[4] Lazzaroni, M.; Citterio, M.; Latorre, S.; Lanza, A.; Spiazzi, G., *Point of Load for LHC experiments: Testing the behaviour in hostile environment*, *Instrumentation and Measurement Technology Conference (I2MTC) Proceedings, 2014 IEEE International*, pp.681-686, 12-15 May 2014

[5] Lazzaroni, M.; Citterio, M.; Latorre, S.; Lanza,A., *High B Test of a commercial step-down Point of Load for LHC experiments*, *Measurement*, Available online 20 October 2014, ISSN 0263-2241

[6] Fuentes, C.; Allongue, B.; Blanchot, G.; Faccio, F.; Michelis, S.; Orlandi, S.; Pontt, J.; Rodriguez, J.; Kayal, M., *Optimization of DC-DC Converters for Improved Electromagnetic Compatibility With High Energy Physics Front-End Electronics*, Nuclear Science, IEEE Transactions on , vol.58, no.4, pp.2024,2031, Aug. 2011

[7] Fuentes, C., *Optimization of the design of DC-DC converters for improving the electromagnetic compatibility with the Front-End electronic for the super Large Hadron Collider Trackers* Ph.D. Dissertation, Universidad Técnica Federico Santa María